Dalton Transactions

Accepted Manuscript

ROYAL SOCIETY OF CHEMISTRY

www.rsc.org/dalton

Albumin binding and ligand-exchange processes of the Ru(III) anticancer agent NAMI-A and its *bis*-DMSO analogue determined by ENDOR spectroscopy

Coordination of Ru(III) anticancer candidates to albumin via histidine imidazoles has been demonstrated by electron nuclear double resonance (ENDOR) spectroscopy.

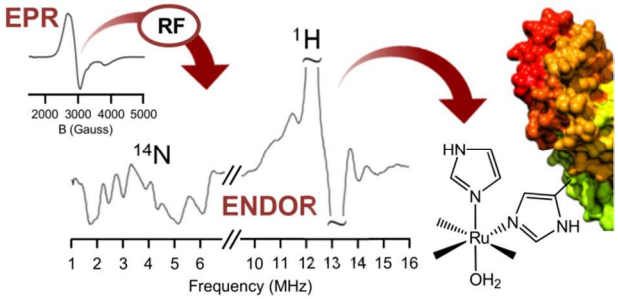

Dalton Transactions

RSCPublishing

ARTICLE

Albumin binding and ligand-exchange processes of the Ru(III) anticancer agent NAMI-A and its *bis*-DMSO analogue determined by ENDOR spectroscopy†

Cite this: DOI: 10.1039/x0xx00000x

Received 00th January 2012,
Accepted 00th January 2012

DOI: 10.1039/x0xx00000x

www.rsc.org/

Michael I. Webb,[a,b*] and Charles J. Walsby[a*]

The ruthenium anticancer compound NAMI-A, imidazolium [*trans*-$RuCl_4$(1*H*-imidazole)(DMSO-*S*)], is currently undergoing advanced clinical evaluation. As with other Ru(III) chemotherapeutic candidates, interactions with human serum albumin (HSA) have been identified as a key component of the speciation of NAMI-A following intravenous administration. To characterize coordination to HSA, we have performed electron paramagnetic resonance (EPR) and electron nuclear double resonance (ENDOR) spectroscopic analysis of deuterium-labelled isotopologues of both NAMI-A and its *bis*-DMSO analogue, $[(DMSO)_2H][$*trans*-$RuCl_4(DMSO\text{-}S)_2]$ (Ru-*bis*-DMSO). Samples were prepared using phosphate buffered saline, in the presence of HSA, and with the individual amino acids histidine, cysteine, and alanine. Analysis of ^{1}H ENDOR spectra shows characteristic hyperfine interactions from DMSO, water, and imidazole ligands. Furthermore, coordination of imidazole ligands was confirmed from diagnostic ^{14}N ENDOR signals. Combined with the EPR data from the complexes following incubation in the presence of histidine, the ENDOR data demonstrate that both complexes bind to HSA via histidine imidazoles. Furthermore, the protein-bound species are shown to have water ligands and, in the case of Ru-*bis*-DMSO, one species has a remaining coordinated DMSO.

Introduction

Ruthenium-based anticancer compounds are currently a major focus of medicinal inorganic chemistry.[1] Diverse activities and low-levels of side effects suggest that ruthenium complexes could have significant advantages over platinum anticancer drugs such as cisplatin, which are amongst the most widely used compounds in modern chemotherapy.[2] Fundamental properties of ruthenium complexes make them particularly attractive as potential anticancer drugs, including: (i) octahedral geometry, which allows for structural diversity and modes of action that are distinct from square-planar Pt(II) complexes, (ii) slow rates of ligand exchange, which are often on the order of cell-division processes,[3] and (iii) a range of oxidation states that are accessible under physiological conditions, specifically 2+, 3+, and 4+.[4] Recent development of ruthenium compounds has been dominated by octahedral Ru(III) coordination complexes and Ru(II) organometallic arene compounds.[1c, 5] The former have advanced the furthest towards clinical application with the most prominent examples being NAMI-A, imidazolium [*trans*-$RuCl_4$(1*H*-imidazole)(DMSO-*S*)] (**Fig. 1**),[6] and the *bis*-indazole complexes KP1019 and NKP-1339 all showing very promising results in clinical trials.[7]

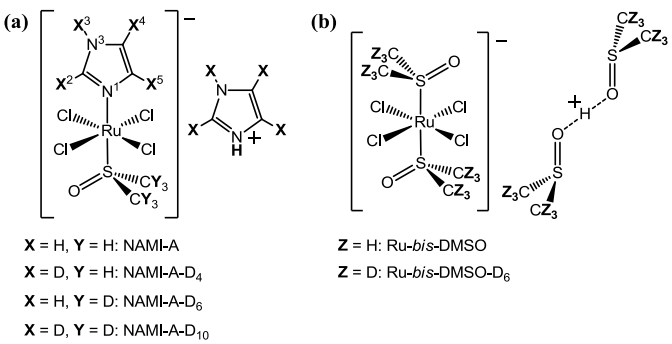

Fig. 1: NAMI-A, Ru-*bis*-DMSO, and their isotopologues used for ENDOR measurements.

NAMI-A inhibits the development and growth of metastases but has widely been considered to be non-cytotoxic.[8] However, it has been reported recently that NAMI-

[a] Department of Chemistry, Simon Fraser University, 8888 University Drive, Burnaby, BC, V5A 1S6, Canada. Email: cwalsby@sfu.ca

[b] Department of Chemistry and Geochemistry, Montana Tech of the University of Montana, 1300 W Park Street, Butte, Montana, 59701, USA. Email: mwebb@mtech.edu

†*Electronic supplementary information (ESI) available. For ESI see DOI: 10.1039/xxxxxxxxx*

A does exhibit selective antiproliferative effects on several leukaemia cell lines.[9] Despite extensive investigation, the origin of the activity of NAMI-A and other Ru(III) chemotherapeutics still remains to be fully established. Previous studies have demonstrated that NAMI-A is not significantly internalized by cells and consequently extracellular processes have been linked to the antimetastatic activity of the complex.[8b, 10] In particular, collagen interactions,[8k, 11] activation of integrin receptors,[8c] and binding to cell membranes[10a, 12] have been implicated. A variety of other Ru-DMSO complexes have been reported to have similar activity profiles to NAMI-A, with relatively low cytotoxicity but good antimetastatic properties, indicating that this is a common feature of such compounds.[8i, 13] In this work, $[(DMSO)_2H][trans\text{-}RuCl_4(DMSO\text{-}S)_2]$ (Ru-*bis*-DMSO) (**Fig. 1**),[14] which is also the synthetic precursor of NAMI-A, has been chosen as an additional representative of these types of compounds and as a spectroscopic reference.

A wide variety of techniques have been used to characterize the ligand exchange processes, protein binding, and cellular interactions of NAMI-A.[10a, 12, 14b, 15] Interactions with human serum albumin (HSA) have been a particular focus of these studies since it is likely a major transporter of NAMI-A *in vivo*.[15k, 16] We have demonstrated previously that electron paramagnetic resonance (EPR) is a useful tool for such studies, since it reports changes to the ligand environments of Ru(III) (low-spin d^5, $S = ½$) complexes. Using this technique, we have inferred the identity of Ru(III) species from spectral features and variation of signal intensities, as determined by deconvolution of the experimental data via simulation. In this report we describe the application of electron nuclear double resonance (ENDOR) spectroscopy to directly characterize the ligand environments of species formed from NAMI-A and Ru-*bis*-DMSO by ligand-exchange processes. ENDOR spectroscopy has been described as "EPR detected NMR", and typically uses microwave radiation to saturate EPR transitions at a selected magnetic field, while simultaneously radiofrequency (RF) radiation is applied.[17] The resulting spectra of RF absorptions are defined by the characteristic Larmor frequency of each nucleus as well as hyperfine and nuclear-electric quadrupolar interactions. These data can thus determine the identity of coordinated nuclei and their interaction with a specific paramagnetic centre.

Using ^1H, ^2H, and ^{14}N ENDOR of NAMI-A, Ru-*bis*-DMSO, and their deuterated derivatives (**Fig. 1**), we have probed the coordination of these complexes to HSA. Comparison of these measurements with the spectra of the complexes in phosphate buffered saline (PBS) and in the presence of individual amino acids has enabled ligand exchange processes and the mode of HSA coordination for each complex to be determined.

Experimental

Synthetic procedures

NAMI-A and Ru-*bis*-DMSO were synthesized according to literature procedures.[18] Isotopically labelled analogues were also synthesized following the same literature procedures with incorporation of D_6-DMSO (99.9%, Cambridge isotope laboratories) and D_4-imidazole (98%, Cambridge isotope laboratories). Each labelled complex was checked for purity using elemental analysis with results as follows: Ru-*bis*-DMSO, Calc. C 17.27 H 4.53 N 0.00, Found C 17.41 H 4.52 N 0.00; Ru-*bis*-DMSO-D_6, Calc. C 16.55 H/D 4.17 N 0.00, Found C 16.51 H/D 4.18 N 0.00; NAMI-A, Calc. C 20.97 H 3.30 N 12.23, Found C 21.16 H 3.29 N 12.08; NAMI-A-D_4 Calc. C 20.61 H/D 3.24 N 12.02, Found C 20.46 H/D 3.31 N 11.69; NAMI-A-D_6 Calc. C 20.70 H/D 3.26 N 12.07, Found C 20.67 H/D 3.20 N 11.69; NAMI-A-D_{10} EA: Calc. C 20.35 H/D 3.20 N 11.86, Found C 20.67, H/D 3.10 N 11.84.[19]

Preparation of EPR and ENDOR Samples

Ru(III) complexes in buffer. For NAMI-A, Ru-*bis*-DMSO, and their isotopologues, 20 mM samples for ENDOR measurements were prepared by dissolving each complex in 150 μL of a PBS solution (pH 7.4) containing 137 mM NaCl, 2.7 mM KCl, 10 mM Na_2HPO_4, and 2 mM KH_2PO_4 followed by the addition 150 μL of glycerol. The samples were mixed, and immediately frozen in liquid nitrogen until use.

Ru-*bis*-DMSO solution behaviour samples. For EPR studies of the solution behaviour of Ru-*bis*-DMSO, samples were prepared by dissolving the complex in PBS (3 mM, 1050 μL) followed by incubation at 37 °C. After 0, 10, 20, 30, and 60 minutes of incubation 210 μL aliquots were drawn from a stock solution and mixed with 90 μL of glycerol and immediately frozen in liquid nitrogen until use.

NAMI-A, Ru-*bis*-DMSO and Ru-*bis*-DMSO-D_6 with HSA. Each Ru(III) complex was dissolved in PBS (20 mM, 600 μL), and immediately mixed with a solution of HSA (2.5 mM, 600 μL) and diluted to a final volume of 4 mL using PBS. The resulting solutions were incubated at 37 °C for 30 minutes, after which protein-bound fractions were isolated using Amicon centrifugal filter units (30 kDa molecular weight cut-off) by centrifuging at 8 °C and 4500 rpm for 30 minutes, or until a volume of less than 200 μL was attained. The filtered product was promptly made up to 210 μL with PBS and mixed with 90 μL of glycerol before being transferred to an EPR tube and frozen in liquid nitrogen until use. A ratio of complex to HSA of 8:1 was used to ensure a maximum concentration of protein coordinated species. The resulting EPR spectra for NAMI-A with HSA were indistinguishable from previous studies using a 2:1 ratio,[15k] indicating that this does not affect the coordination mode. The relatively high concentrations of NAMI-A, as compared to likely *in vivo* concentrations, used in these studies were required to produce sufficient signal-to-noise in the ENDOR experiments.

NAMI-A and Ru-*bis*-DMSO with amino acids. Each Ru(III) complex was dissolved in PBS (10 mM, 1050 μL). The individual amino acids (alanine, cysteine, and histidine) were added (10 mM) to each Ru(III) solution, resulting in a 1:1 ratio of Ru to each amino acid. Each solution was then incubated for 0, 10, 20, 30, and 60 minutes at 37 °C, and up to 120 minutes

for NAMI-A with histidine. Subsequently, 210 μL fractions were taken and mixed with 90 μL of glycerol and immediately frozen in liquid nitrogen until use.

EPR Measurements and Simulations

EPR spectra were collected at X-band (~9.5 GHz) using a Bruker EMXplus spectrometer with a PremiumX microwave bridge and HS resonator. Measurements were performed at 20 K using a Bruker ER 4112HV helium temperature-control system and continuous-flow cryostat. Sample volumes were 300 μL and reproducible placement of sample tubes within the quartz insert tube holder ensured that variation in instrument sensitivity between measurements was minimal, and automatic tuning of the spectrometer gave a Q-factor of 6700 ± 5%. EPR spectra were simulated using the program Bruker WinEPR Simfonia and a manual, iterative fitting procedure was used to deconvolute contributions from overlapping spectra when multiple Ru(III) species were present in a particular sample. The g values determined from these simulations are shown in **Table 1**, and the line widths are also shown in **Table S1**.

ENDOR Measurements

Continuous wave (CW) ENDOR measurements were performed using the same Bruker EMXplus spectrometer used for EPR measurements, but operating with a Bruker DICE-ENDOR system with a EN 801 CW resonator and 150 Watt Bruker CW RF amplifier. This system produces first-derivative spectral lines.

EPR Experimental Conditions

All of the time-course EPR spectra were measured using the same experimental conditions, in order to facilitate comparisons between data sets. The conditions used were: frequency = 9.38 GHz, microwave power = 2.0 mW, time constant = 40.96 msec, modulation amplitude = 6 Gauss, average of five 2-minute scans, measurement temperature = 20 K.

ENDOR Experimental Conditions

ENDOR experiments were conducted with the following parameters: modulation frequency = 25 kHz, modulation amplitude = 0 Gauss, microwave power = 31.7 mW, frequency = 9.47 GHz, time constant = 1.28 ms, RF modulation depth = 250 kHz, RF attenuation = 6 db, average of 100 five-second scans. All samples were measured at 20 K.

Interpretation of ENDOR spectra

For a nucleus (N) with spin I = ½ interacting with a paramagnetic centre with S = ½, the first-order ENDOR spectrum from a single molecular orientation is given by:

$$\nu_{\pm} = |\nu_N \pm \frac{A}{2}| \qquad (1)$$

which corresponds to a doublet of lines centred at the Larmor frequency, ν_N, and split by the hyperfine coupling constant A, when $\nu_N > A/2$. Such ENDOR splitting patterns are observed for ^{1}H nuclei in this study. For nuclei with I > ½, additional splittings from nuclear-electric quadrupole interactions may also be observed, resulting in spectral lines that to first-order are given by:

$$\nu_{\pm}(\pm) = |\nu_N \pm \frac{A}{2} \pm \frac{3P}{2}| \qquad (2)$$

where P is the orientation-dependent nuclear-electric quadrupole splitting. In the case of ^{2}H nuclei (I = 1), hyperfine and quadrupole splitting are typically small and are rarely resolved in CW ENDOR experiments. Furthermore, since $\nu_N > A/2$, the ^{2}H spectra are centred at the Larmor frequency. In the case of larger hyperfine couplings, as often observed for ^{14}N nuclei (I = 1), it is possible for $A/2 > \nu_N$, in which case equation 2 describes a spectrum that is centred at A/2 and split by $2\nu_N$.

Results

Ru-*bis*-DMSO in PBS

Ru-*bis*-DMSO was incubated in PBS at 37 °C for time periods up to 60 minutes and EPR data were collected to study ligand exchange processes and for ENDOR analysis. After the complex was dissolved in PBS at room temperature and immediately frozen, the so-called "0 time point", a uniaxial EPR spectrum from a single species was observed ($g_\perp$ = 2.43, $g_{||}$ = 1.77) (**Fig. 2 (inset)**). ENDOR spectra from this first time point were collected at both $g_\perp$ and $g_{||}$. For the unlabelled complex this revealed several well-resolved ^{1}H hyperfine splittings around the proton Larmor frequency at both fields (**Fig. 2(a)**). Some weak signals were also observed at low frequency (2.5 – 4 MHz), which may originate from chlorine ligands (^{35}Cl, I = 3/2, 75.78%, ^{37}Cl, I = 3/2, 24.22%).

The ^{1}H ENDOR signals at $g_\perp$ indicate different types of ligand protons due to multiple hyperfine splittings. EPR measurements of the complex with deuterated DMSO (Ru-*bis*-DMSO-D_6) in PBS showed the same spectrum as the unlabelled compound (**Fig. S3(b)**). However, a pair of sharp peaks with $A(^1H)$ = 1.8 MHz are absent in the ^{1}H ENDOR (**Fig. 2(b)**), demonstrating that these resonances arise from DMSO protons. Coordination of the deuterated ligand was demonstrated by the observation of a strong low-frequency peak, which is close to the ^{2}H Larmor frequency at this field ($\nu(^2H)$ = 1.8 MHz). Additionally, signals from more strongly coupled protons, $A(^1H)$ = 3.9 MHz, were still present in the ^{1}H ENDOR spectrum of Ru-*bis*-DMSO-D_6. Dissolution of the deuterated complex in D_2O/PBS left the EPR spectrum unchanged (**Fig. S3(c)**) but supressed these ^{1}H ENDOR signals while leaving a strong ^{2}H ENDOR signal (**Fig. 2(c)**). This demonstrates that the strongly coupled proton signal originated from a coordinated water ligand. A relatively intense ^{1}H signal around $A(^1H) \sim 0$ from Ru-*bis*-DMSO-D_6 in PBS is primarily from "distant" solvent matrix protons.[20] A small contribution from this signal can also be seen from Ru-*bis*-DMSO-D_6 in D_2O/PBS due to a low concentration of H_2O derived from the buffering agents,

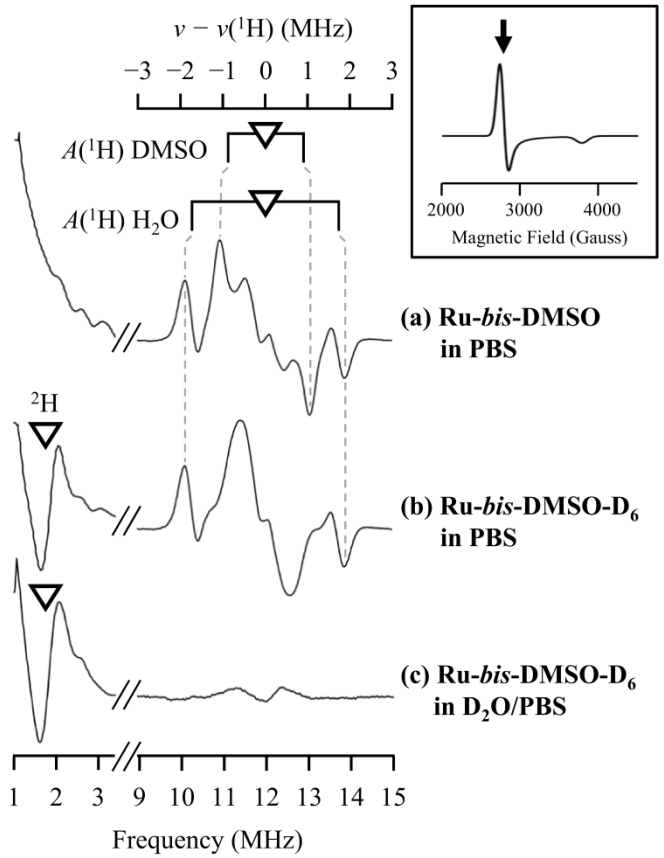

Fig. 2, Main panel: ENDOR spectra from (**a)** Ru-*bis*-DMSO in PBS, (**b)** Ru-*bis*-DMSO-D_6 in PBS, (**c)** Ru-*bis*-DMSO-D_6 in D_2O/PBS, measured at $g_\perp$. **Inset:** EPR spectrum of Ru-*bis*-DMSO in PBS with ENDOR field indicated by arrow. Hyperfine couplings marked at derivative turning points. Dashed lines indicate peaks of derivative line shapes for comparison of spectral features.

Na_2HPO_4 and KH_2PO_4, and possibly small amounts of atmospheric H_2O mixing with the D_2O solution over time.[21]

At $g_\parallel$, Ru-*bis*-DMSO and Ru-*bis*-DMSO-D_6 also show water protons with strong couplings that are not visible when the deuterated complex is dissolved in D_2O. At this field the water resonances are split, with peaks at 3.0 and 4.6 MHz around $\nu(^1H)$ (**Fig. S7**), which is due to a dipolar component of the hyperfine interactions.[17a] That this is visible at $g_\parallel$ but not $g_\perp$ is a consequence of field-dependent orientation selection, which splits the perpendicular and parallel components of the hyperfine interaction.[17d, 22] Signals from DMSO are not resolved at $g_\parallel$ and, based on signal intensities, this is likely due to smaller splittings at this field leading to overlap with the distant proton signal near $A(^1H) = 0$. Overall, the ^1H ENDOR data demonstrate that the species in solution at "time 0" is not the parent compound Ru-*bis*-DMSO, but rather the mono-aqua complex formed by a single DMSO exchange (Ru-DMSO-H_2O).

The observation of a uniaxial EPR spectrum at the shortest incubation time point is also consistent with formation of the tetragonal Ru-DMSO-H_2O complex following DMSO exchange. With further incubation at 37 °C changes in the EPR spectra reflect new species generated by further ligand-exchange processes (**Fig. S1**). Analysis of spectral components at incubation times up to 60 minutes reveals contributions from two additional species (**Fig. S2**). The first has a rhombic spectrum g = [2.40, 2.24, 1.89] and is thus assigned to the low symmetry species $RuCl_3$(DMSO-*S*)$(H_2O)_2$ (Ru-$(H_2O)_2$-eq) formed by loss of a chloride ligand from Ru-DMSO-H_2O. A second species with a uniaxial EPR spectrum ($g_\perp$ = 2.35, $g_\parallel$ = 1.80) becomes increasingly predominant at longer incubation times and, based on the implied tetragonal symmetry of the complex, is consistent with formation of the di-aqua complex via aqueous ligand exchange with the remaining DMSO ligand of Ru-DMSO-H_2O to give [*trans*-$RuCl_4(H_2O)_2]^-$ (Ru-$(H_2O)_2$-ax). These, and other assignments of EPR spectra (*vide infra*) are made assuming that secondary coordination sphere effects are not significant.[23] Changes in the EPR signals with incubation in PBS were accompanied by a darkening of the solution from bright yellow-orange to dark brown. This has been observed previously in the solution behaviour of NAMI-A, and is thought to arise from the formation of dimers or oligomers of the aquated Ru complex.[13a, 15c]

NAMI-A in PBS

NAMI-A has a uniaxial EPR spectrum ($g_\perp$ = 2.47, $g_\parallel$ = 1.72) (**Fig. 3 (inset)**) consistent with the tetragonal symmetry of the complex.[17b] ENDOR measurements of unlabelled NAMI-A at $g_\perp$ revealed well-defined spectral features in both the ^1H region and below 7 MHz (**Fig. 3**). The signals at low frequency are consistent with ^{14}N nuclei (I = 1, 99.63%) from the imidazole ligand of NAMI-A. This assignment can be made confidently given the intensity of the signals, the lack of other spin-bearing nuclei, and the absence of similar signals in the ENDOR spectrum of Ru-*bis*-DMSO (**Fig. 4**). The CW ENDOR system used for these studies produces derivative mode spectra and is not optimized for measuring low frequency signals. This difficulty is compounded by the likely overlap between the ^{14}N ENDOR signals of N^1 and N^3 of the imidazole ring (**Fig. 1**), isotropic and dipolar contributions to the hyperfine interaction, and orientation selection effects.[17a, 22] Thus, any assignment of specific peaks is preliminary, and we have tentatively indicated possible peak assignments at $g_\perp$ for N^1 corresponding to an A/2 centred spectrum, with $A(^{14}N)$ = 8 MHz and a quadrupole splitting of 0.8 MHz (**Fig. 3**).

Deuterium labelling of NAMI-A has no significant effect on the EPR spectra (**Fig. S3(d)–(h)**), but does lead to distinct changes in the ^1H ENDOR (**Fig. 3**). The unlabelled complex shows a complex lineshape due to the overlap of proton signals from both the DMSO and imidazole ligands. Deuteration of the imidazole ligand simplifies the ^1H ENDOR pattern to reveal a pair of sharp peaks that match the signals from DMSO protons observed for Ru-*bis*-DMSO, with similar line shapes and hyperfine coupling of $A(^1H)$ = 1.8 MHz. These peaks are supressed in the spectrum of the complex with deuterated DMSO (NAMI-A-D_6) confirming that they originate from the

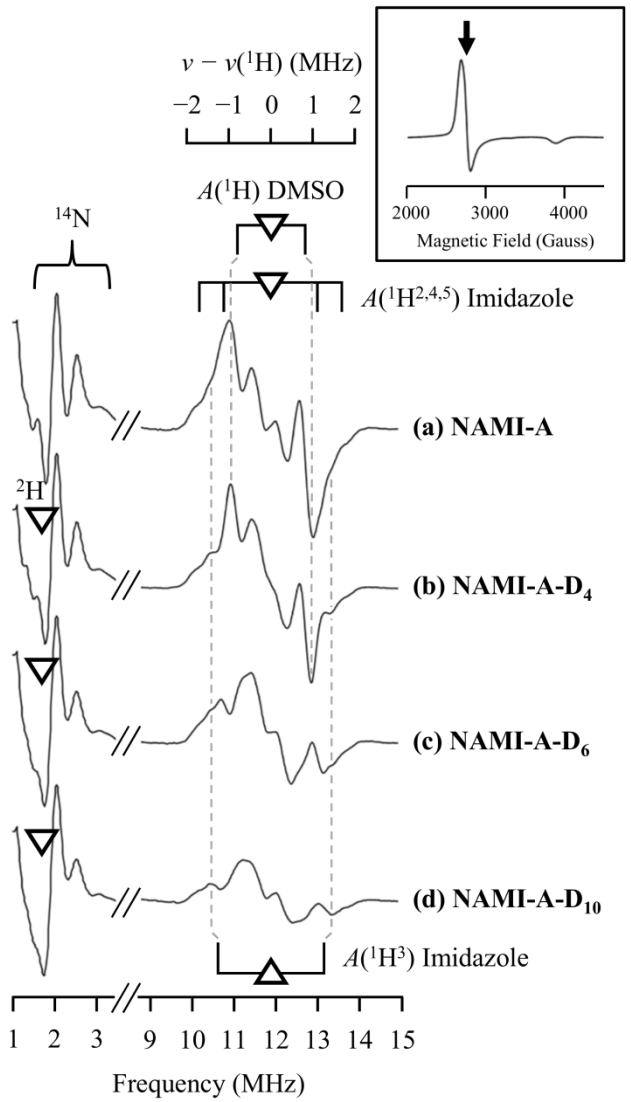

Fig. 3, Main Panel: ^{1}H ENDOR of NAMI-A and its deuterated derivatives in PBS, measured at $g_\perp$. **Inset:** EPR spectrum of NAMI-A in PBS with ENDOR field indicated by arrow. Hyperfine couplings marked at derivative turning points. Dashed lines indicate peaks of derivative line shapes for comparison of spectral features.

coordinated DMSO ligand. Consequently, the more strongly coupled ^{1}H signals ($A(^1H)$ = 2.2 MHz) in this spectrum are derived from the four imidazole protons. This is confirmed by the spectrum of the fully labelled complex, NAMI-A-D_{10}, which shows a single remaining strongly coupled proton signal ($A(^1H)$ = 2.6 MHz) arising from the exchangeable proton H^3 of the imidazole ring. Although this signal looks similar to that from NAMI-A-D_6, the signal intensity is significantly lower and the peaks are identifiable as a component of the overlapping peaks from all of the imidazole protons (see guidelines in **Fig. 3**). As with Ru-*bis*-DMSO, signal intensity around $A(^1H)$ = 0 is derived from coupling to distant solvent protons. ENDOR signals from ^{2}H nuclei cannot be resolved for the labelled NAMI-A complexes since they overlap with the signals from ^{14}N, but do cause small systematic changes to the shape of the low frequency region (**Fig. 3**).

When the magnetic field was set to $g_\parallel$, the effects of deuterium labelling on the ^{1}H ENDOR spectral features are less clear, due to peak overlaps (**Fig. S12**). However, reduction in ^{1}H signal intensity with increasing inclusion of ^{2}H is observed.

Table 1: g values of the observed Ru(III) species determined from simulation of EPR spectra

Species	g_1	g_2	g_3
Ru- DMSO-H_2O	2.43	2.43	1.77
Ru-$(H_2O)_2$-eq	2.40	2.24	1.89
Ru-$(H_2O)_2$-ax	2.35	2.35	1.80
Ru-HSA-1	2.40	2.40	1.72
Ru-HSA-2	2.50	2.25	1.10
Ru-HSA-3	2.42	2.05	1.88
Ru-His-1	2.37	2.37	1.82
Ru-His-2	2.40	2.40	1.77
NAMI-A	2.47	2.47	1.72
NAMI-A-H_2O	2.30	2.30	1.88
NAMI-A-HSA-1	2.43	2.43	1.76
NAMI-A-HSA-2	2.54	2.26	1.76
NAMI-A-HSA-3	2.42	2.06	1.96
NAMI-A-His	2.52	2.29	1.78

Interactions with HSA

Ru-*bis*-DMSO with HSA

Incubation of Ru-*bis*-DMSO with HSA for 30 minutes at 37 °C gives a broad EPR signal indicating a change in the ligand environment of the Ru(III) centre, which is consistent with coordination to the protein (**Fig. 4(b)**). Spectral deconvolution by simulation (**Fig. S13(a)**) shows that this spectrum is comprised of two broad signals, one of which is uniaxial (Ru-HSA-1, $g_\perp$ = 2.40, $g_\parallel$ = 1.72) and the other rhombic (Ru-HSA-2, g = [2.50, 2.25, 1.10]). A minor, sharp signal from a third species was also observed (g = [2.42, 2.05, 1.88]). Similar species have been reported in previous EPR studies of the binding of NAMI-A to HSA, with the broad signals suggested to be from protein coordination via histidine imidazoles.[15k] As with NAMI-A, the uniaxial signal from Ru-*bis*-DMSO binding to HSA was assigned to a species with tetragonal local symmetry from protein coordination at an axial position previously occupied by DMSO in Ru-*bis*-DMSO, and the rhombic signal to complexes bound to an equatorial position following chloride dissociation.

After Ru-*bis*-DMSO was incubated with HSA for 30 minutes at 37 °C, the resulting EPR spectrum was well simulated using only components from protein coordinated species (**Fig. S13(a)**). Consequently, ENDOR signals are also only from protein bound complexes, with no significant contributions from Ru-DMSO-H_2O or other aquated species. ENDOR data were collected at g = 2.3, which is at the maximum slope in the $g_\perp/g_1$ region of the two overlapping

broad EPR signals from the HSA-coordinated species. (**Fig. 4(b)**). Broad, low intensity EPR signals at $g_{\|}$ or g_3 of these species meant that ENDOR measurements at these fields did not produce sufficient signal-to-noise for analysis. Comparison of the low frequency ENDOR region (below 7 MHz) from Ru-*bis*-DMSO in PBS (**Fig. 4(a)**) with that of the complex with HSA (**Fig. 4(b)**) clearly shows several new resonances. These are consistent with ^{14}N hyperfine interactions and quadrupole splittings, as expected from coordination of a histidine imidazole. This assignment is reinforced by noting that the low frequency ENDOR line splittings are reminiscent of those observed for NAMI-A (**Fig. 3**), consistent with coordinated imidazole ligands in both cases.

The ^1H ENDOR spectrum of Ru-*bis*-DMSO with HSA shows couplings matching those previously assigned to DMSO (1.8 MHz) and water (3.7 MHz) ligands for the complex in PBS (**Fig. 4**). Furthermore, when the deuterated complex Ru-*bis*-DMSO-D_6 was incubated with HSA, the EPR spectrum was unchanged (**Fig. 4(c), inset**), but ^1H ENDOR signals corresponding to DMSO ligands were suppressed (**Fig. 4(c)**). In the absence of the ^1H signals from coordinated DMSO, two additional proton peaks with couplings of 2.2 MHz were revealed (**Fig. 4(c)**). These signals are assigned to protons from a coordinated histidine imidazole since they have couplings similar to those from the imidazole ligand of NAMI-A (**Fig. 3**). As expected, the ^{14}N ENDOR signals from Ru-*bis*-DMSO-D_6 were the same as the unlabelled complex, but interfered with observation of ^2H signals from coordinated DMSO-D_6. Strong distant ^1H ENDOR signals for the complexes in the presence of HSA, which were not observed in PBS only, may indicate contributions from protons in the local protein environment of the coordinated complexes.

NAMI-A with HSA

As described above, we have previously used EPR to characterize coordination of NAMI-A to HSA.[15k] After 30 minutes of incubation at 37 °C, a broad spectrum (**Fig. 5(b)**) composed of a uniaxial component (NAMI-A-HSA-1, $g_{\perp} = 2.43$ and $g_{\|} = 1.76$) and a rhombic component (NAMI-A-HSA-2, g = [2.54, 2.26, 1.76]) (**Fig. S13(c)**), were observed. A minor contribution from a third rhombic species was also observed (NAMI-A-HSA-3, g = [2.42, 2.06, 1.96]), however the identity of this species was not determined. ENDOR spectra were collected at the average of the highest g values of the two main species (g = 2.36), while signal intensity was not sufficient for analysis in the $g_{\|}/g_3$ region. Analysis of the low frequency region of the ENDOR spectrum from NAMI-A with HSA was impeded by the potential overlap of ^{14}N signals from the imidazoles of both the original complex and histidine side chains. As shown in **Fig. 5**, the spectral data below 7 MHz for NAMI-A and the HSA-bound complexes show distinct differences, consistent with coordination of a second imidazole from histidine. However, as described above, detailed analysis of the ^{14}N ENDOR data in this work is preliminary.

Similar to Ru-*bis*-DMSO, the proton ENDOR show resonances consistent with coordinated imidazole and water with couplings of 2.2 MHz and 3.6 MHz respectively (**Fig.**

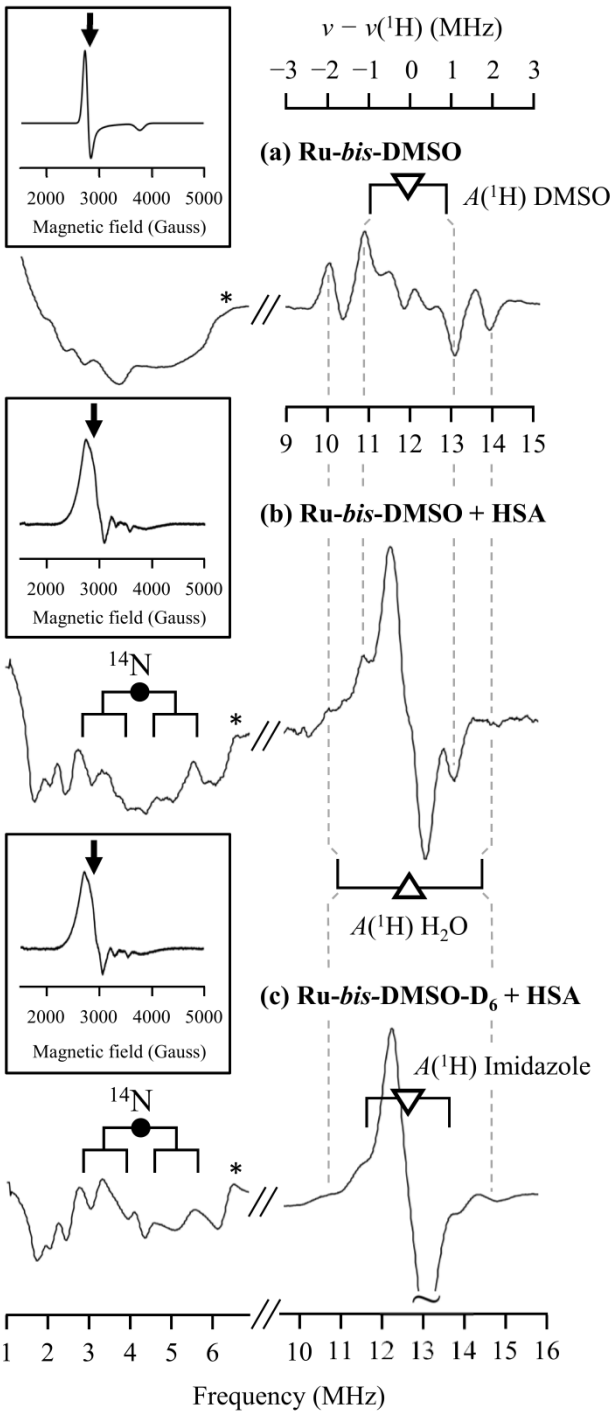

Fig. 4, Main panel: ENDOR spectra from (**a)** Ru-*bis*-DMSO in PBS, (**b)** Ru-*bis*-DMSO with HSA in PBS after incubation at 37 °C for 30 mins, (**c)** Ru-*bis*-DMSO-D_6 with HSA in PBS after incubation at 37 °C for 30 mins, measured at $g_{\perp}$. **Insets:** Corresponding EPR spectra with ENDOR fields indicated by arrows. "*" indicates a 2nd amplifier harmonic from the ^1H signal. Hyperfine couplings marked at derivative turning points. Dashed lines indicate peaks of derivative line shapes for comparison of spectral features.

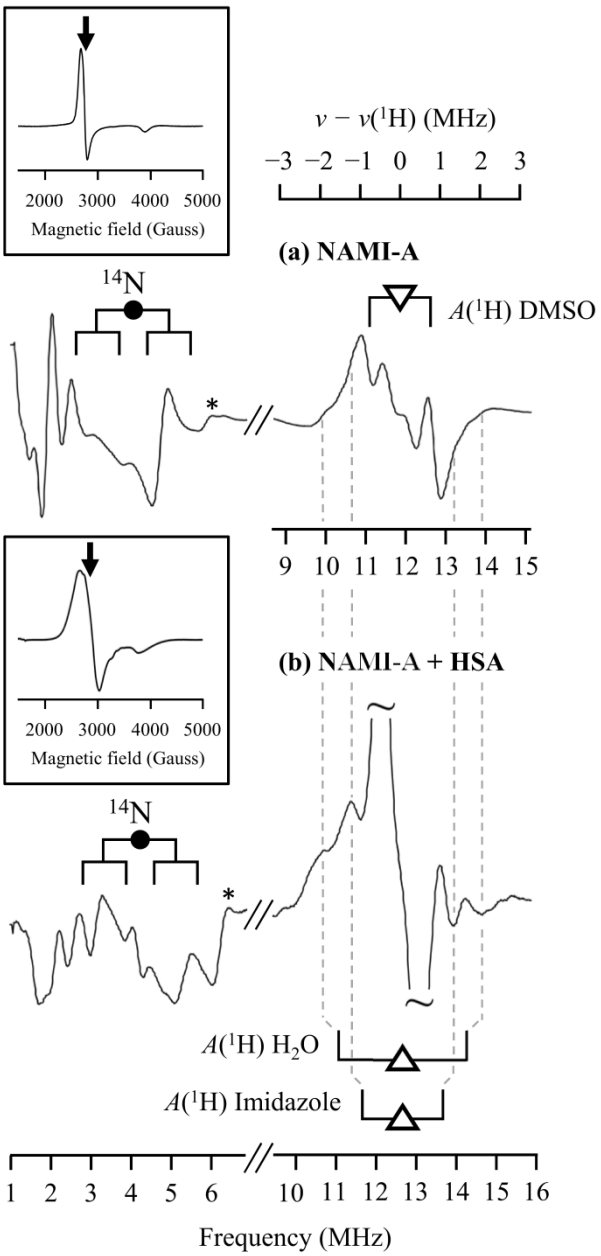

Fig. 5, Main panel: ENDOR spectra from (**a)** NAMI-A in PBS, (**b)** NAMI-A with HSA in PBS after incubation at 37 °C for 30 minutes, measured at $g_{\perp}$. **Insets:** Corresponding EPR spectra with ENDOR fields indicated by arrows. "*" indicates a 2nd amplifier harmonic from the ^{1}H signal. Hyperfine couplings marked at derivative turning points. Dashed lines indicate peaks of derivative line shapes for comparison of spectral features.

5(b)). Furthermore, the absence of peaks with couplings of around 1.8 MHz indicates that neither of the HSA-coordinated species have DMSO ligands.

Interactions with Individual Amino Acids

Ru-*bis*-DMSO with amino acids

When Ru-*bis*-DMSO was incubated with alanine and cysteine (**Fig. S14(a,b)**), the EPR spectra were similar to those of the free complex in solution. This was confirmed by spectral simulation (**Figs S15, S16**), which demonstrated that the solution behaviour of the complex was unaffected by the presence of these amino acids. Furthermore, the solution darkened from a bright yellow to dark brown, as observed for the complex in buffer alone, reflecting the formation of oligomeric species.

After incubation of Ru-*bis*-DMSO with histidine, the EPR spectra show features that are not observed from the complex in buffer alone (**Fig. S14(c)**). Spectral deconvolution by simulation (**Fig. 6(a) inset**, **Fig. S17**) determined that these spectral changes are due to the presence of two new species, Ru-His-1 ($g_{\perp}$ = 2.37 and $g_{\parallel}$ = 1.82) and Ru-His-2 ($g_{\perp}$ = 2.40 and $g_{\parallel}$ = 1.77). The uniaxial EPR spectra observed indicate coordination of histidine at an axial ligand position, via ligand exchange with Ru-DMSO-H_2O to give species with either DMSO or water ligands at the second axial ligand position. With increasing incubation, the EPR spectra from these species became increasingly prominent with a concomitant reduction in the signal from Ru-DMSO-H_2O.

ENDOR measurements confirm histidine coordination, principally through the observation of resonances from ^{14}N nuclei at low frequency (**Fig. 6(a)**). With the magnetic field set at the maximum slope of the overlapping $g_{\perp}$ signals from Ru-His-1 and Ru-His-2 (g = 2.37) the ENDOR data below 7 MHz are very similar to those observed for NAMI-A, reflecting coordinated imidazole ligands from histidine. Similar correlations between NAMI-A and Ru-His in the ^{14}N data are also observed in the $g_{\parallel}$ region (g = 1.82, **Fig. S18**). The ^{1}H ENDOR data at g = 2.37 (**Fig. 6(a)**) contain contributions from four Ru(III) species in solution at this incubation time point. Consequently strong signals from coordinated DMSO and water ligands are evident. However, in addition, two additional resonances that appear as shoulders with couplings of ~2.6 MHz are also visible. These correlate with the ^{1}H hyperfine couplings from the coordinated imidazole of NAMI-A (**Fig. 3**) and are consistent with the coordinated histidine imidazoles of Ru-His-1 and Ru-His-2.

NAMI-A with amino acids

NAMI-A was also incubated with individual amino acids in an effort to identify the residue responsible for HSA coordination. The EPR spectra of the alanine and cysteine samples (**Fig. S19(a,b)**) are essentially indistinguishable from NAMI-A following incubation in PBS. After 30 minutes, only signals from the parent complex and the mono-aqua derivative formed by exchange of the axial DMSO ligand, NAMI-A-H_2O, are observed in each case, which was confirmed by simulation (**Figs S20, S21**).

The EPR spectrum following incubation of NAMI-A with histidine is similar at early time points to the complex in buffer. However, after 30 minutes of incubation, a new broad signal is observed, and becomes increasingly predominant at later time points (**Fig. 6(b) inset**, **Fig. S22**), although the overall signal intensity is low. From spectral simulations (**Fig. S22**), this new

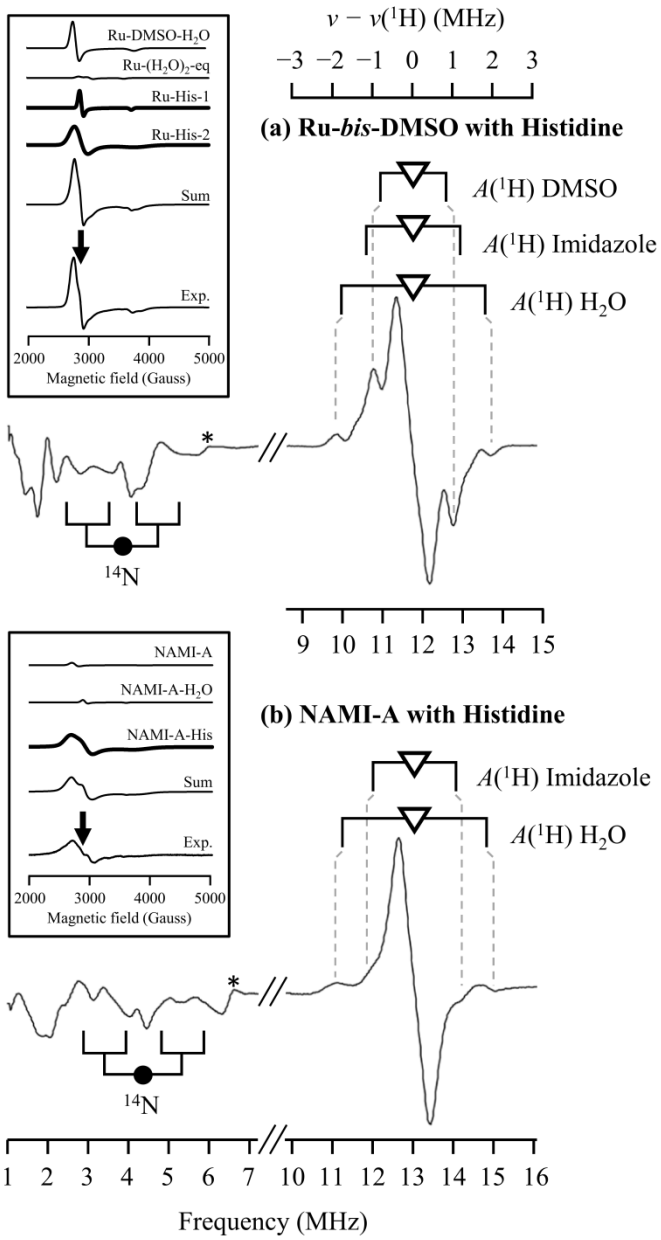

Fig. 6, Main panel: ENDOR spectra from (**a)** Ru-*bis*-DMSO with histidine in PBS after incubation at 37 °C for 30 mins, **(b)** NAMI-A with histidine in PBS after incubation at 37 °C for 120 mins, measured at $g_{\perp}$. **Insets:** Corresponding EPR spectra with ENDOR fields indicated by arrows. "*" indicates a 2nd amplifier harmonic from the ^{1}H signal. Hyperfine couplings marked at derivative turning points. Dashed lines indicate peaks of derivative line shapes for comparison of spectral features.

species, NAMI-A-His, has spectral parameters (g = [2.52, 2.29, 1.78]) very similar to those of the HSA-coordinated species NAMI-A-HSA-2 (g = [2.54, 2.26, 1.76].[15k]

ENDOR spectra were measured with the magnetic field set at the average of the high-field g values of NAMI-A-His, $(g_{1}+g_{2})/2$ = 2.41, (**Fig. 6(b)**). In the ^{1}H ENDOR spectrum, couplings from coordinated imidazole (~2.1 MHz) and water (3.6 MHz) ligands are observed, but resonances from DMSO are not apparent. In the region below 7 MHz, signals consistent with ^{14}N are visible and have shapes that are distinct from those observed for NAMI-A, as expected given that the presence of a second imidazole ligand from histidine in the case of NAMI-A-His. However, as described above, such assignments are preliminary given the data available.

Discussion

Application of the ENDOR Technique

Under physiological conditions Ru(III) anticancer complexes can undergo multiple ligand exchange processes, which has contributed to the current uncertainty as to the active species *in vivo*. A variety of techniques have been used to address this problem,[10a, 14b, 15a-j, 24] including our previous application of EPR, to provide insight into the solution behaviour of Ru(III) complexes such as NAMI-A.[12, 15k, 25] In our EPR studies "powder pattern" spectra from frozen solutions were analysed in terms of the spectral shapes as defined by g values and line widths. While this approach has proven to be very useful, the identity of various Ru(III) species in solution was inferred from the order they were produced in solution after incubation for different intervals, and from symmetry arguments. More specific characterization of these species can, in principle, be obtained from hyperfine interactions between the paramagnetic Ru(III) centre and spin-bearing nuclei of the coordinated ligands. However, line splittings from these interactions are not observed in the EPR spectra due to large intrinsic line widths and overlap from the ensemble of orientation-dependent spectra that make up the observed powder patterns. This information can be recovered using ENDOR spectroscopy, since this technique can resolve single-crystal-like hyperfine structures from randomly-oriented paramagnetic systems.[17] These hyperfine interactions can then potentially provide atomic-level details of the coordination environment around the paramagnetic metal centre. ENDOR has been applied to characterize the coordination sphere of a variety of systems including metal complexes, defect centres in solids, and metalloenzymes.[17, 26]

Surprisingly, ENDOR studies of Ru(III) species are almost unknown in the literature.[27] Thus, the studies reported herein are a new approach to characterizing Ru(III) anticancer compounds. The CW ENDOR system used in this work produces derivative mode spectra which works well for ^{1}H ENDOR, but is not optimal for measuring broad, low-frequency signals such as from ^{14}N nuclei. This, combined with overlapping signals from both nitrogens of each imidazole, has limited us to a preliminary interpretation of the ^{14}N hyperfine patterns. More detailed analysis of the hyperfine and quadrupole interactions from coordinated ^{14}N nuclei may be possible in the future using pulsed ENDOR methods combined with spectral simulations.

ENDOR of parent compounds and ligand exchange processes

The use of deuterated derivatives of NAMI-A and Ru-*bis*-DMSO has enabled their ^{1}H ENDOR hyperfine interactions to be fully assigned. In the case of NAMI-A this confirmed the previous assignment of the EPR spectrum from the parent compound.[15k] However, for Ru-*bis*-DMSO it was determined that the uniaxial EPR spectrum observed after minimal incubation in PBS was actually the first aquation product, Ru-DMSO-H_2O, formed by exchange of a DMSO ligand. This is consistent with a previous report that Ru-*bis*-DMSO rapidly releases one of its DMSO ligands upon dissolution in water.[14a] Comparison with the relatively slow exchange rate for the second DMSO ligand, and for the DMSO exchange of NAMI-A, demonstrates the importance of the axial ligands on ligand-exchange rates for these types of complexes, and reflects the destabilizing *trans* effect of *S*-bonded DMSO ligands.[28]

A key result of the measurements of the complexes in PBS is the value of the ^{1}H hyperfine couplings for the DMSO, H_2O, and imidazole ligands. Importantly, the size of these couplings is very specific to the particular ligands so that, for example, the ^{1}H hyperfine coupling for DMSO in the $g_{\perp}/g_1$ region from NAMI-A, Ru-DMSO-H_2O, and Ru-*bis*-DMSO with HSA are identical within experimental error. Furthermore, comparison of the low frequency regions shows that NAMI-A has strong signals that are not visible for Ru-DMSO-H_2O. This enables ^{14}N resonances from the imidazole of NAMI-A to be assigned unequivocally. These data then serve as a reference for the expected couplings to imidazole ligands from HSA and isolated histidine.

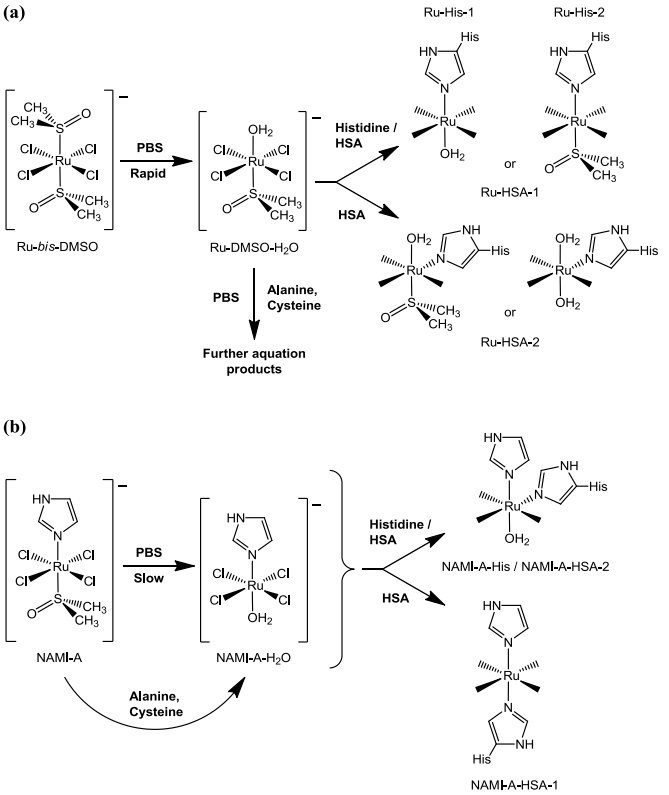

Fig. 7 Ligand exchange processes for **(a)** Ru-*bis*-DMSO and **(b)**, NAMI-A as determined by EPR and ENDOR. For the complexes in the presence of histidine and HSA, only ligands directly detected by ENDOR are shown.

Interactions with HSA

Human serum albumin is the most common protein in the circulatory system and is a well-established transporter of endogenous and exogenous species, including pharmaceuticals.[29] Consequently, interactions of Ru chemotherapeutics with HSA have been a focus of numerous studies. Messori *et al*. originally demonstrated that both NAMI-A and the sodium compensated analogue of Ru-*bis*-DMSO formed adducts with bovine serum albumin (BSA), using UV-Vis and circular dicroism spectroscopies.[15h] It has now been established using a variety of methods that NAMI-A binds readily to HSA.[15k, 16c-e, 30] Initial studies of adducts of NAMI-A with BSA demonstrated significantly reduced activity, which was attributed to reduced bioavailability.[16a] However, subsequent reports have suggested that BSA[31] and HSA[16d] adducts retain the anitmetastatic activity of the parent compound.

The specific mode of NAMI-A binding to HSA has previously been hypothesized to occur via coordination to histidine imidazoles, but direct evidence for this has not been reported. Histidine coordination has been suggested by UV-Vis studies of NAMI-A with BSA in which the histidine sidechains of the protein were modified by diethylpyrocarbonate.[15h] Furthermore, X-ray absorption spectroscopy (XAS) studies show coordination of nitrogen donor ligands in the presence of BSA.[31] We have previously used EPR to characterise both non-coordinate and coordinate interactions of NAMI-A with HSA.[15k] The dominant EPR signals produced by coordinated species have large line widths, which may indicate multiple histidine binding sites, each of which has a somewhat different chemical environment.

To our knowledge, there is one report of the X-ray crystallographic characterization of a Ru(III) anticancer related complex coordinated to HSA. In this instance $[RuCl_5(ind)]^{2-}$ was shown to coordinate at two sites; at one via histidine, and at another with histidine and lysine.[32] Similarly, the structure of KP1019 with the structurally similar protein lactoferrin demonstrates histidine coordination.[33] Two X-ray crystal structures of NAMI-A adducts with other proteins have been reported. The first of these studies characterized binding to human carbonic anhydrase II, indicating two sites of Ru coordination, involving a histidine imidazole or alternatively the carbonyl oxygen atom of an asparagine and the peptidic nitrogen of a histidine.[34] A second study of NAMI-A with hen egg white lysozyme (HEWL) shows mono-dentate coordination of Ru to the side-chain carboxylates of aspartic acid residues.[35] Surprisingly, a similar study of the pyridine analogue of NAMI-A, pyridinium [*trans*-$RuCl_4$(1*H*-pyridine)(DMSO-*S*)] (AziRu), with HEWL shows different behaviour, with a single binding

site involving Ru coordination to a histidine imidazole and a carboxylate oxygen of aspartic acid.[36] A related study of AziRu with RNase A shows two histidine imidazole binding sites.[37]

While these reports demonstrate some diversity in the coordination modes of NAMI-A-type complexes with proteins, they do demonstrate that histidine coordination is favourable. Interestingly, each of these studies also show that all of the original NAMI-A ligands are lost in the process of protein coordination and are replaced either by amino acid or water ligands. This contrasts with our analysis using EPR and ENDOR spectroscopy, suggesting that crystal soaking experiments may produce different results from solution studies.

The ENDOR studies presented here provide direct evidence for HSA coordination via histidine imidazoles. In the case of Ru-*bis*-DMSO the appearance of resonances in the low-frequency region following incubation with HSA shows the coordination of nitrogen ligands unequivocally, since no other protein nuclei can give such signals. That these signals arise from histidine coordination is indicated by ^{14}N hyperfine and quadrupole patterns that are similar to those observed for NAMI-A, consistent with a coordinated imidazole ligand in each case. Additionally, imidazole ^{1}H ENDOR signals, assigned by comparison with hyperfine couplings from labelled NAMI-A, are observed from Ru-*bis*-DMSO coordinated to HSA. More subtle differences in the ^{14}N line shapes between NAMI-A and Ru-*bis*-DMSO coordinated to HSA may be due to the presence of two protein-coordinated species, Ru-HSA-1 and Ru-HSA-2, which were identified by EPR (**Fig. 7(a)**). Overlap of the distinct ^{14}N ENDOR signals from these two species gives an overall signal that differs from NAMI-A, but nonetheless has similar spectral parameters.

Since ENDOR data from Ru-*bis*-DMSO were collected after 30 minutes of incubation with HSA, a time point at which the EPR signals are essentially only from protein-coordinated species, the ENDOR spectra are from Ru-HSA-1 and Ru-HSA-2. Thus, the observation of ^{1}H signals from DMSO and H_2O ligands demonstrates that these ligands are part of the coordination sphere of the HSA-coordinated species (**Fig. 7(a)**). However, because the ^{1}H ENDOR signals are derived from two different coordinated Ru(III) species with overlapping EPR spectra, it is not possible to assign the H_2O or DMSO ligand coordination specifically to either of the individual HSA-coordinated species.

In the case of NAMI-A, interpretation of the ^{14}N ENDOR from protein coordinated species is less definitive due to the imidazole ligand of the parent complex. However, there are distinct differences in the low frequency regions, which are consistent with the coordination of a second imidazole ligand from histidine. As we have reported previously, EPR spectra from two species reflecting axial and equatorial protein coordination modes are observed by EPR. The ^{1}H ENDOR signals from these species demonstrate that H_2O ligands are present, but that no DMSO ligands are coordinated (**Fig. 7(b)**).

Interactions with individual amino acids

Recently, Vergara *et al.* have surveyed X-ray crystal structures of Ru(II) and Ru(III) protein adducts deposited in the protein data bank.[37] In 13 of the 16 reports they have listed, histidine coordination is described, demonstrating that this is a predominant site of ruthenium binding to proteins in either of the physiologically relevant oxidation states. However, coordination to the side chains of other amino acids has also been reported frequently, including nitrogen coordination from lysine, the oxygen donors of glutamine, aspartic acid, asparagine, and cysteine thiolates.

To gain more insight into the amino acid residues responsible for the coordination of Ru-*bis*-DMSO and NAMI-A to HSA and other proteins, we incubated each complex with alanine, cysteine, and histidine. As described above, the EPR and ENDOR spectra of the complexes with alanine and cysteine are very similar to those in PBS alone, indicating no coordination of the amino acids. This is consistent with the thiolate and amino groups having pKa values sufficiently high, such that they are not significantly deprotonated at pH 7.4. By contrast the lower pKa of the histidine imidazole (pKa = 6.0) means it will be deprotonated at physiological pH, promoting coordination to Ru(III).

The observation of two new EPR signals when Ru-*bis*-DMSO is incubated with histidine indicates two species, Ru-His-1 and Ru-His-2, involving coordination to the amino acid. ^{14}N and ^{1}H ENDOR signals confirm histidine imidazole coordination and the similarity of these signals to those of the HSA coordinated complex also indicate that this is the mode of protein coordination. Due to overlapping EPR signals (**Fig. 6(a)**), ^{1}H ENDOR from DMSO and H_2O do not specify which of these ligands is coordinated at the axial positions of Ru-His-1 and Ru-His-2. However, this can be inferred from their EPR spectra. Given that both species have uniaxial EPR spectra, indicating a tetragonal coordination environment, imidazole coordination at an axial position is required. Furthermore, since these species are derived from Ru-DMSO-H_2O, the other axial ligand is either DMSO or water. Since the g values of Ru-His-1 ($g_\perp$ = 2.37 and $g_\parallel$ = 1.82) are closer to the first aquation product of NAMI-A (NAMI-A-H_2O, $g_\perp$ = 2.30 and $g_\parallel$ = 1.88) that forms after exchange of the axial DMSO ligand, this species likely has an axial water ligand also (**Fig. 7 (a)**). Consequently, the second species Ru-His-2, likely has an axial DMSO ligand. Significantly, the g values and line widths of Ru-His-2 ($g_\perp$ = 2.40 and $g_\parallel$ = 1.77) are very similar to those of the protein bound species Ru-HSA-1 ($g_\perp$ = 2.40 and $g_\parallel$ = 1.72), indicating similar coordination environments, with axial DMSO and histidine imidazole ligands in both cases.

EPR spectra of NAMI-A with histidine also reveal a new species with a rhombic EPR spectrum. The g values of this species are very similar to those of NAMI-A-HSA-2 suggesting coordination of the histidine imidazole at an equatorial position previously occupied by chloride. Differences in the ^{14}N region of the ENDOR spectrum compared to NAMI-A also provide direct evidence for histidine coordination. Furthermore, the

absence of DMSO signals in the ^{1}H ENDOR demonstrates that none of the species in solution, including the histidine coordinated complex, have DMSO ligands (**Fig. 7(b)**).

Conclusions

Due to a variety of ligand exchange processes that are possible *in vivo*, NAMI-A and other Ru(III) complexes such as Ru-*bis*-DMSO are well described as pro-drugs. HSA-bound species are likely to be predominant *in vivo* and thus identifying these species is a critical part of understanding the mechanism of action for these compounds. In this report we have used ENDOR and EPR spectroscopy to demonstrate that NAMI-A and Ru-*bis*-DMSO coordinate to HSA via histidine imidazoles, and have also identified H_2O and DMSO ligation to protein coordinated species. Comparison with isolated histidine has provided further confirmation of these coordination modes. Overall, these studies provide insight into the interactions of Ru(III) anticancer complexes with HSA and demonstrate that ENDOR spectroscopy is a useful tool for establishing specific details of the ligand exchange processes of these types of compounds.

Abbreviations

EPR	Electron paramagnetic resonance
ENDOR	Electron nuclear double resonance
RF	Radio frequency
CW	Continuous wave
PBS	Phosphate buffered saline
HSA	Human serum albumin
BSA	Bovine serum albumin
Ru-*bis*-DMSO	$[(DMSO)_2H][trans\text{-}RuCl_4(DMSO\text{-}S)_2]$
Ru-DMSO-H_2O	$[trans\text{-}RuCl_4(DMSO\text{-}S)(H_2O)]^-$
Ru-$(H_2O)_2$-eq	$RuCl_3(DMSO\text{-}S)(H_2O)_2$
Ru-$(H_2O)_2$-ax	$[trans\text{-}RuCl_4(H_2O)_2]^-$
Ru-HSA-1,2,3	HSA coordinated species derived from Ru-*bis*-DMSO
Ru-His-1,2	Histidine coordinated species derived from Ru-*bis*-DMSO
NAMI-A	Imidazolium [*trans*-$RuCl_4$(1*H*-imidazole)(DMSO-*S*)]
NAMI-A-H_2O	$[trans\text{-}RuCl_4(1H\text{-imidazole})(H_2O)]^-$
NAMI-A-HSA-1,2,3	HSA coordinated species derived from NAMI-A
NAMI-A-His	Histidine coordinated species derived from NAMI-A

Acknowledgements

The authors would like to thank Paul Mulyk for assistance with measurement and interpretation of elemental analysis. Financial support was provided by The Natural Sciences and Engineering Research Council of Canada (NSERC), through an NSERC Discovery grant to CJW and an NSERC PGS D award to MIW.

References

1. a) M. J. Clarke, *Coord. Chem. Rev.*, 2003, **236**, 209-233; b) M. A. Jakupec, M. Galanski, V. B. Arion, C. G. Hartinger and B. K. Keppler, *Dalton Trans.*, 2008, 183-194; c) A. Levina, A. Mitra and P. A. Lay, *Metallomics*, 2009, **1**, 458-470; d) E. S. Antonarakis and A. Emadi, *Cancer Chemother. Pharmacol.*, 2010, **66**, 1-9; e) E. Alessio, G. Mestroni, A. Bergamo and G. Sava, *Met. Ions Biol. Syst.*, 2004, **42**, 323-351.
2. C. X. Zhang and S. J. Lippard, *Curr. Opin. Chem. Biol.*, 2003, **7**, 481-489.
3. J. Reedijk, *Platinum Met. Rev.*, 2008, **52**, 2-11.
4. C. S. Allardyce and P. J. Dyson, *Platinum Met. Rev.*, 2001, **45**, 62-69.
5. a) A. Bergamo and G. Sava, *Dalton Trans.*, 2011, **40**, 7817-7823; b) Y. K. Yan, M. Melchart, A. Habtemariam and P. J. Sadler, *Chem. Commun.*, 2005, 4764-4776; c) W.-H. Ang, A. Casini, G. Sava and P. J. Dyson, *J. Organomet. Chem.*, 2011, **696**, 989-998.
6. a) E. Alessio, G. Mestroni, A. Bergamo and G. Sava, *Curr. Top. Med. Chem.*, 2004, **4**, 1525-1535; b) J. M. Rademaker-Lakhai, D. Van Den Bongard, D. Pluim, J. H. Beijnen and J. H. M. Schellens, *Clin. Cancer Res.*, 2004, **10**, 3717-3727.
7. a) C. G. Hartinger, S. Zorbas-Seifried, M. A. Jakupec, B. Kynast, H. Zorbas and B. K. Keppler, *J. Inorg. Biochem.*, 2006, **100**, 891-904; b) S. Kapitza, M. Pongratz, M. A. Jakupec, P. Heffeter, W. Berger, L. Lackinger, B. K. Keppler and B. Marian, *J. Cancer Res. Clin. Oncol.*, 2005, **131**, 101-110; c) R. Trondl, P. Heffeter, C. R. Kowol, M. A. Jakupec, W. Berger and B. K. Keppler, *Chem. Sci.*, 2014, **5**, 2925-2932.
8. a) M. Bacac, M. Vadori, G. Sava and S. Pacor, *Cancer Immunol. Immunother.*, 2004, **53**, 1101-1110; b) A. Bergamo, M. Cocchietto, I. Capozzi, G. Mestroni, E. Alessio and G. Sava, *Anti-Cancer Drugs*, 1996, **7**, 697-702; c) A. Bergamo and G. Sava, *Dalton Trans.*, 2007, 1267-1272; d) M. Cocchietto, S. Zorzet, A. Sorc and G. Sava, *Invest. New Drugs*, 2003, **21**, 55-62; e) F. Frausin, V. Scarcia, M. Cocchietto, A. Furlani, B. Serli, E. Alessio and G. Sava, *J. Pharmacol. Exp. Ther.*, 2005, **313**, 227-233; f) B. Gava, S. Zorzet, P. Spessotto, M. Cocchietto and G. Sava, *J. Pharmacol. Exp. Ther.*, 2006, **317**, 284-291; g) S. Pacor, S. Zorzet, M. Cocchietto, M. Bacac, M. Vadori, C. Turrin, B. Gava, A. Castellarin and G. Sava, *J. Pharmacol. Exp. Ther.*, 2004, **310**, 737-744; h) G. Pintus, B. Tadolini, A. M. Posadino, B. Sanna, M. Debidda, F. Bennardini, G. Sava and C. Ventura, *Eur. J. Biochem.*, 2002, **269**, 5861-5870; i) G. Sava, E. Alessio, A. Bergamo and G. Mestroni, *Top. Biol. Inorg. Chem.*, 1999, **1**, 143-169; j) G. Sava, K. Clerici, I. Capozzi, M. Cocchietto, R. Gagliardi, E. Alessio, G. Mestroni and A. Perbellini, *Anti-Cancer Drugs*, 1999, **10**, 129-138; k) G. Sava, S. Zorzet, C. Turrin, F. Vita, M. Soranzo, G. Zabucchi, M. Cocchietto, A. Bergamo, S. DiGiovine, G. Pezzoni, L. Sartor and S. Garbisa, *Clin. Cancer Res.*, 2003, **9**, 1898-1905; l) S. Zorzet, A. Bergamo, M. Cocchietto, A. Sorc, B. Gava, E. Alessio, E. Iengo and G. Sava, *J. Pharmacol. Exp. Ther.*, 2000, **295**, 927-933; m) S. Zorzet, A. Sorc, C. Casarsa, M. Cocchietto and G. Sava, *Met.-Based Drugs*, 2001, **8**, 1-7.
9. S. Pillozzi, L. Gasparoli, M. Stefanini, M. Ristori, M. D'Amico, E. Alessio, F. Scaletti, A. Becchetti, A. Arcangeli and L. Messori, *Dalton Trans.*, 2014, **43**, 12150-12155.

10. a) J. B. Aitken, S. Antony, C. M. Weekley, B. Lai, L. Spiccia and H. H. Harris, *Metallomics*, 2012, **4**, 1051-1056; b) A. Bergamo, C. Gaiddon, J. H. M. Schellens, J. H. Beijnen and G. Sava, *J. Inorg. Biochem.*, 2012, **106**, 90-99.
11. G. Sava, F. Frausin, M. Cocchietto, F. Vita, E. Podda, P. Spessotto, A. Furlani, V. Scarcia and G. Zabucchi, *Eur. J. Cancer*, 2004, **40**, 1383-1396.
12. M. I. Webb and C. J. Walsby, *Metallomics*, 2013, **5**, 1624-1633.
13. a) G. Mestroni, E. Alessio, G. Sava, S. Pacor and M. Coluccia, in *Metal Complexes in Cancer Chemotherapy*, ed. B. K. Keppler, VCH, Weinheim, 1993, pp. 157-185; b) I. Bratsos, S. Jedner, T. Gianferrara and E. Alessio, *Chimia*, 2007, **61**, 692-697; c) A. Bergamo and G. Sava, *Dalton Trans.*, 2007, 1267-1272.
14. a) E. Alessio, G. Balducci, M. Calligaris, G. Costa, W. M. Attia and G. Mestroni, *Inorg. Chem.*, 1991, **30**, 609-618; b) J. S. Jaswal, S. J. Rettig and B. R. James, *Can. J. Chem.*, 1990, **68**, 1808-1817.
15. a) S. Antony, J. B. Aitken, S. Vogt, B. Lai, T. Brown, L. Spiccia and H. H. Harris, *J. Biol. Inorg. Chem.*, 2013, **18**, 845-853; b) I. Ascone, L. Messori, A. Casini, C. Gabbiani, A. Balerna, F. Dell'Unto and A. Congiu Castellano, *Inorg. Chem.*, 2008, **47**, 8629-8634; c) M. Bacac, A. C. G. Hotze, K. van der Schilden, J. G. Haasnoot, S. Pacor, E. Alessio, G. Sava and J. Reedijk, *J. Inorg. Biochem.*, 2004, **98**, 402-412; d) J. Chen, L. Chen, S. Liao, K. Zheng and L. Ji, *J. Phys. Chem. B*, 2007, **111**, 7862-7869; e) M. Groessl, O. Zava and P. J. Dyson, *Metallomics*, 2011, **3**, 591-599; f) A. Levina, J. B. Aitken, Y. Y. Gwee, Z. J. Lim, M. Liu, A. M. Singharay, P. F. Wong and P. A. Lay, *Chem. - Eur. J.*, 2013, **19**, 3609-3619; g) O. Mazuryk, K. Kurpiewska, K. Lewinski, G. Stochel and M. Brindell, *J. Inorg. Biochem.*, 2012, **116**, 11-18; h) L. Messori, P. Orioli, D. Vullo, E. Alessio and E. Iengo, *Eur. J. Biochem.*, 2000, **267**, 1206-1213; i) M. Sooriyaarachchi, J. L. Wedding, H. H. Harris and J. Gailer, *JBIC, J. Biol. Inorg. Chem.*, 2014, **19**, 1049-1053; j) A. V. Vargiu, A. Robertazzi, A. Magistrato, P. Ruggerone and P. Carloni, *J. Phys. Chem. B*, 2008, **112**, 4401-4409; k) M. I. Webb and C. J. Walsby, *Dalton Trans.*, 2011, **40**, 1322-1331.
16. a) A. Bergamo, L. Messori, F. Piccioli, M. Cocchietto and G. Sava, *Invest. New Drugs*, 2003, **21**, 401-411; b) M. Brindell, I. Stawoska, J. Supel, A. Skoczowski, G. Stochel and R. Eldik, *JBIC, J. Biol. Inorg. Chem.*, 2008, **13**, 909-918; c) M. Groessl, E. Reisner, C. G. Hartinger, R. Eichinger, O. Semenova, A. R. Timerbaev, M. A. Jakupec, V. B. Arion and B. K. Keppler, *J. Med. Chem.*, 2007, **50**, 2185-2193; d) V. Novohradsky, A. Bergamo, M. Cocchietto, J. Zajac, V. Brabec, G. Mestroni and G. Sava, *Dalton Trans.*, 2015, **44**, 1905-1913; e) M. Ravera, S. Baracco, C. Cassino, D. Colangelo, G. Bagni, G. Sava and D. Osella, *J. Inorg. Biochem.*, 2004, **98**, 984-990.
17. a) J. Telser, in *Encyclopedia of Inorganic and Bioinorganic Chemistry*, John Wiley & Sons, Ltd, 2011; b) J. A. Weil and J. R. Bolton, *Electron paramagnetic resonance: elementary theory and practical applications*, 2nd edn., Wiley-Interscience, Hoboken, N.J., 2007; c) B. M. Hoffman, *Acc. Chem. Res.*, 2003, **36**, 522-529; d) D. M. Murphy and R. D. Farley, *Chem. Soc. Rev.*, 2006, **35**, 249-268.
18. a) E. Alessio, G. Balducci, A. Lutman, G. Mestroni, M. Calligaris and W. M. Attia, *Inorg. Chim. Acta*, 1993, **203**, 205-217; b) *United States Pat.*, 6,221,905, 2001.
19. For deuterated compounds the H/D quantification has been corrected to account for the instrumental report of deuterium.
20. a) J. Lambe, N. Laurance, E. C. McIrvine and R. W. Terhune, *Phys. Rev.*, 1961, **122**, 1161-1170; b) J. S. Hyde, G. H. Rist and L. E. G. Eriksson, *J. Phys. Chem.*, 1968, **72**, 4269-4276.
21. J. W. Ellis and B. W. Sorge, *J. Chem. Phys.*, 1934, **2**.
22. P. E. Doan, *ACS Symp. Ser.*, 2003, **858**, 55-81.
23. M. L. Souza, E. E. Castellano, J. Telser and D. W. Franco, *Inorg. Chem.*, 2015, **54**, 2067-2080.
24. a) A. R. Timerbaev, C. G. Hartinger, S. S. Aleksenko and B. K. Keppler, *Chem. Rev.*, 2006, **106**, 2224-2248; b) K.-G. Lipponer, E. Vogel and B. K. Keppler, *Met.-Based Drugs*, 1996, **3**, 243-260; c) M. Groessl, C. G. Hartinger, P. J. Dyson and B. K. Keppler, *J. Inorg. Biochem.*, 2008, **102**, 1060-1065; d) M. Groessl, C. G. Hartinger, A. Egger and B. K. Keppler, *Metal Ions in Biology and Medicine*, 2006, **9**, 111-116; e) A. Kung, T. Pieper and B. K. Keppler, *J. Chromatogr. B*, 2001, **759**, 81-89; f) K. Polec-Pawlak, K. Abramski Jan, J. Ferenc, S. Foteeva Lidia, R. Timerbaev Andrei, K. Keppler Bernhard and M. Jarosz, *J. Chromatogr. A*, 2008, **1192**, 323-326; g) A. R. Timerbaev, A. V. Rudnev, O. Semenova, C. G. Hartinger and B. K. Keppler, *Analytical Biochemistry*, 2005, **341**, 326-333; h) M. Pongratz, P. Schluga, M. A. Jakupec, V. B. Arion, C. G. Hartinger, G. Allmaier and B. K. Keppler, *J. Anal. At. Spectrom.*, 2004, **19**, 46-51.
25. N. Cetinbas, M. I. Webb, J. A. Dubland and C. J. Walsby, *J. Biol. Inorg. Chem.*, 2010, **15**, 131-145.
26. B. M. Hoffman, *Acc. Chem. Res.*, 1991, **24**, 164-170.
27. P. Doan, N. Lees, M. Shanmugam and B. Hoffman, *Appl Magn Reson*, 2010, **37**, 763-779.
28. a) J. A. Davies, *Adv. Inorg. Chem. Radiochem.*, 1981, **24**, 115-187; b) Q. A. De Paula, A. A. Batista, O. R. Nascimento, A. J. Da Costa-Filho, M. S. Schultz, M. R. Bonfadini and G. Oliva, *J. Braz. Chem. Soc.*, 2000, **11**, 530-536.
29. a) B. Elsadek and F. Kratz, *J. Controlled Release*, 2012, **157**, 4-28; b) F. Kratz, *J. Controlled Release*, 2008, **132**, 171-183; c) T. Peters, *Adv. Protein Chem.*, 1985, **37**, 161-245.
30. I. Khalaila, A. Bergamo, F. Bussy, G. Sava and P. J. Dyson, *Int. J. Oncol.*, 2006, **29**, 261-268.
31. M. M. Liu, Z. J. Lim, Y. Y. Gwee, A. Levina and P. A. Lay, *Ang. Chem. Int. Ed.*, 2010, **49**, 1661-1664.
32. Y. Zhang, A. Ho, J. Yue, L. Kong, Z. Zhou, X. Wu, F. Yang and H. Liang, *Eur. J. Med. Chem.*, 2014, **86**, 449-455.
33. E. N. Baker, B. F. Anderson, H. M. Baker, H. R. Faber, C. A. Smith and A. J. Sutherland-Smith, in *Exp. Biol. Med. (Totowa, N. J.)*, Humana, 1997, vol. 28, pp. 177-191.
34. A. Casini, C. Temperini, C. Gabbiani, C. T. Supuran and L. Messori, *ChemMedChem*, 2010, **5**, 1989-1994.
35. L. Messori and A. Merlino, *Dalton Trans.*, 2014, **43**, 6128-6131.
36. A. Vergara, G. D'Errico, D. Montesarchio, G. Mangiapia, L. Paduano and A. Merlino, *Inorg. Chem.*, 2013, **52**, 4157-4159.
37. A. Vergara, I. Russo Krauss, D. Montesarchio, L. Paduano and A. Merlino, *Inorg. Chem.*, 2013, **52**, 10714-10716.

